Inorg. Chem. **2003**, *42*, 4469–4478

Photoluminescence Properties of Four-Coordinate Gold(I)–Phosphine Complexes of the Types $[Au(diphos)_2]PF_6$ and $[Au_2(tetraphos)_2](PF_6)_2$

Christopher D. Delfs,[†] Heather J. Kitto,[§] Robert Stranger,[†] Gerhard F. Swiegers,*[,‡] S. Bruce Wild,[§] Anthony C. Willis,[§] and Gerard J. Wilson[‡]

Department of Chemistry, The Faculties, Australian National University, Canberra, Australian Capital Territory 0200, Australia, Division of Molecular Science, Commonwealth Scientific and Industrial Research Organization (CSIRO), Bag 10, Clayton South, Victoria 3169, Australia, and Research School of Chemistry, Australian National University, Canberra, Australian Capital Territory 0200, Australia

Received November 13, 2002

Numerous reports describe the photoluminescence of two- and three-coordinate gold(I)–phosphine complexes, but emission in their analogous four-coordinate complexes is almost unknown. This work examines the luminescence of tetrahedral gold(I) complexes of the types $[Au(diphos)_2]PF_6$ (diphos = 1,2-bis(diphenylphosphino)ethane, **1**) and $[Au_2(tetraphos)_2](PF_6)_2$ (tetraphos = (*R**,*R**)-(±)/(*R**,*S**)-1,1,4,7,10,10-hexaphenyl-1,4,7,10-tetraphosphadecane, (*R**,*R**)-(±)/(*R**,*S**)-**2**). Although nonemitting in solution, these complexes luminesce with an intense yellow color (λ_{max} 580–620 nm) at 293 K in the solid state or when immobilized as molecular dispersions within solid matrixes. The excited-state lifetimes of the emissions (τ 4.1–9.4 μs) are markedly dependent on the inter- and intramolecular phenyl–phenyl pairing interactions present. At 77 K in an ethanol glass, two transitions are observed: a minor emission at λ_{max} 415–450 nm and a major emission at λ_{max} 520–595 nm. For $[Au(\mathbf{1})_2]PF_6$, lifetimes of τ 251.0 ± 20.5 μs were determined for the former transition and τ 14.9 ± 4.6 μs for the latter. Density functional theory (DFT) calculations and comparative studies indicate that the former of these emissions involves triplet LMCT π^*(Ph) → Au(d)–P(p) transitions associated with individual *P*-phenyl groups. The latter emissions, which are the only ones observed at 293 K, are assigned to LMCT π^*(Ph–Ph) → Au(d)–P(p) transitions associated with excited *P*-phenyl dimers. Other tetrahedral gold(I)–phosphine complexes containing paired *P*-Ph substituents display similar emissions. The corresponding phosphine ligands, whether free, protonated, or bound to Ag(I), do not exhibit comparable emissions. Far from being rare, luminescence in four-coordinate Au(I)–phosphine complexes appears to be general when stacked *P*-phenyl groups are present.

Introduction

Although many two- and three-coordinate gold(I)−phosphine complexes exhibit luminescence properties,[1] only one four-coordinate gold(I)−phosphine complex and a derivative thereof have been reported to be emissive.[2] The complexes $[Au(\mathbf{3a})_2]PF_6$ and $[Au(\mathbf{3b})_2]PF_6$ (Scheme 1), which contain tetrahedral four-coordinate gold(I) centers, produce intense emissions when irradiated at their respective UV absorption maxima, both in solution and in the solid state. At 298 K in the solid state, they display broad emissions with λ_{max} 640−693 nm with excited-state lifetimes of τ 3.2 μs for $[Au(\mathbf{3a})_2]PF_6$ and τ 1.3 μs for $[Au(\mathbf{3b})_2]PF_6$. The mechanism of this luminescence was considered to involve a spin-forbidden $\sigma \rightarrow \pi^*$ (naphthalene) transition closely associated with the electronic structure of the ligand. Other four-coordinate gold(I) compounds, including the related compound $[Au(\mathbf{3c})_2]PF_6$, are nonemissive in the solid state and solution.[3]

In recent work, we separated the diastereomers and resolved the racemate of the conformationally flexible chelating tetra(tertiary phosphine) (*R**,*R**)-(±)/(*R**,*S**)-

* To whom correspondence should be addressed. E-mail: gerry.swiegers@csiro.au.
[†] Department of Chemistry, Australian National University.
[‡] Commonwealth Scientific and Industrial Research Organization.
[§] Research School of Chemistry, Australian National University.

(1) Gade, L. H. *Angew. Chem., Int. Ed. Engl.* **1997**, *36*, 1171 and references therein.
(2) Yam, V. W.-W.; Chan, C.-L.; Choi, S. W.-K.; Wong, K. M.-C.; Cheng, E. C.-C.; Yu, S.-C.; Chan, W.-K.; Cheung, K.-K. *Chem Commun.* **2000**, *53* and references therein.
(3) McCloskey, T. M.; Gray, H. B. *Inorg. Chem.* **1992**, *31*, 1733 and references therein.

10.1021/ic0206701 CCC: $25.00
Published on Web 06/10/2003

Scheme 1

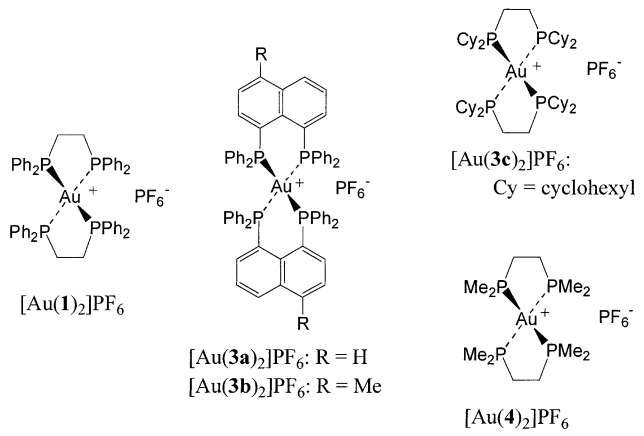

Scheme 2

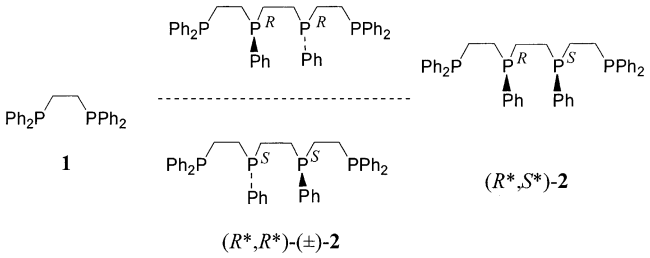

1,1,4,7,10,10-hexaphenyl-1,4,7,10-tetraphosphadecane, (*R**,*R**)-(±)/(*R**,*S**)-**2** (tetraphos)(Scheme 2).[4] When treated with gold(I), diastereomers and enantiomers of the tetraphosphine spontaneously form double-stranded digold(I) complexes of the type $[Au_2(\mathbf{2})_2](PF_6)_2$.[5] In the crystalline solid state, the cations in the complexes adopt a unique *parallel* helical architecture in which the two ligands of the same configuration form single-handed spirals down each side of the metal−metal axis (Figure 1a).[6−8] The parallel helicate appears to be in equilibrium with the double α-helical conformer (Figure 1b) in solution.[5]

The twelve phenyl groups arranged around the metal−metal axis of the helicates generate unusual physical properties. For example, the resulting lipophilicity imbues them with potent antitumor characteristics; these appear to involve a mechanism of action unlike that of conventional anti-cancer agents.[9] We have now discovered that the phenyl groups in the complexes also induce a unique photoluminescence related to *P*-phenyl stacking in concert with the Au(I) ions.

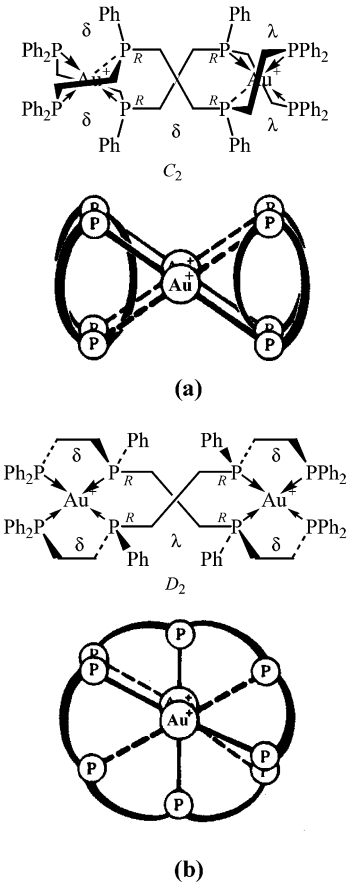

Figure 1. Side-on (top) and end-on (bottom) schematic illustrations of the (a) parallel helical and (b) double-α-helical conformers of (−)-$[Au_2\{(R,R)\text{-}\mathbf{2}\}_2](PF_6)_2$. The parallel helical conformer is present in the crystalline solid state. Molecular mechanics calculations indicate that the double-α-helical rotamer is of similar energy.

This work describes an investigation of the emissive properties of the digold(I) complexes of *tetraphos* and the closely related mononuclear *diphos* complex $[Au(\mathbf{1})_2]PF_6$ (**1** = diphos = 1,2-bis(diphenylphosphino)ethane). Density functional theory (DFT) calculations, along with comparative studies involving the separated diastereomers and enantiomers of the digold(I) complexes, have been used to elucidate the mechanism of the emission.

Experimental Section

Materials. 1,1,4,7,10,10-Hexaphenyl-1,4,7,10-tetraphoshadecane, (*R**,*R**)-(±)/(*R**,*S**)-**2**, was prepared and separated into its constituent diastereomers and enantiomers according to the previously reported procedure.[4,5] The enantiomers (−)-$[Au_2\{(R,R)\text{-}\mathbf{2}\}_2](PF_6)_2$ and (+)-$[Au_2\{(S,S)\text{-}\mathbf{2}\}_2](PF_6)_2$ were prepared as described in ref 5. The optimized synthesis and full characterization of the complex

(4) Airey, A. L.; Swiegers, G. F.; Willis, A. C.; Wild, S. B. *J. Chem. Soc., Chem. Commun.* **1995**, 693.

(5) (a) Airey, A. L.; Swiegers, G. F.; Willis, A. C.; Wild, S. B. *J. Chem. Soc., Chem. Commun.* **1995**, 695. (b) Airey, A. L.; Swiegers, G. F.; Willis, A. C.; Wild, S. B. *Inorg. Chem.* **1997**, *36*, 1588 and references therein. (c) Cook, V. C. PhD Thesis, Australian National University, Canberra, Australia, 2000, pp 133−137.

(6) The structural motif of the *parallel* helicate mimics that of the leucine or zipper transcriptional proteins wherein two polypeptide α-helices are held together by hydrogen bonding in a parallel, side-by-side arrangement. For other self-assembled motifs in coordination chemistry, see Swiegers, G. F.; Malefetse, T. J. *Chem. Rev.* **2000**, *100*, 3483.

(7) We have recently prepared a hexa(tertiary phosphine) that also forms parallel helicates of this type: (a) Bowyer, P. K.; Cook, V. C.; Gharib-Naseri, N.; Gugger, P. A.; Rae, A. D.; Swiegers, G. F.; Willis, A. C.; Zank, J.; Wild, S. B. *Proc. Natl. Acad. Sci. U.S.A.* **2002**, *99*, 4877. (b) Airey, A. L.; Bowyer, P. K.; Cook, V. C.; Naseri, N. G.; Swiegers, G. F.; Willis, A. C.; Wild, S. B. *Phosphorus, Sulfur Silicon Relat. Elem.* **1999**, *146*, 285.

(8) For a comprehensive review of helicates, see: Piguet, C.; Bernardinelli, G.; Hopfgartner, G. *Chem. Rev.* **1997**, *97*, 2005.

(9) The lipophilicity of the helicates appears to cause them to accumulate within the mitochondrial membranes of cells where they have a potent cytotoxic action. The cytotoxicity appears to arise from disruptions to the mitochondrial membrane potentials: McKeage, M. J.; Papathanasiou, P.; Salem, G.; Sjaarda, A.; Swiegers, G. F.; Waring, P.; Wild, S. B. *Met.-Based Drugs* **1998**, *5*, 217. For further information on this topic, see: Berners-Price, S. J.; Sadler, P. J. *Struct. Bonding (Berlin)* **1988**, *70*, 27.

$[Au(\mathbf{1})_2]PF_6$ will be described elsewhere;[10] the preparation of $[Au(\mathbf{1})_2]PF_6$ has been reported previously, but characterization details were not provided.[11,1211,12] Me_2SAuCl was prepared as described previously.[13]

Cast films of poly(methyl methacrylate) (PMMA) were prepared by dissolving known weights of PMMA and the complexes in dichloromethane. Once dissolution was complete, the clear solutions were deposited on glass slides, and the solvent was, in each case, allowed to slowly evaporate under an upturned watch-glass. Clear, transparent PMMA films containing the emitters were subsequently removed from the slides.

Instrumentation. Luminescence spectra were obtained using a Perkin-Elmer LS50 luminescence spectrometer. UV−visible spectra were measured using a Cary 61 instrument. NMR spectra were determined on a Bruker AC200 instrument operating at a proton frequency of 200 MHz. Elemental analyses were carried out by the Campbell Microanalytical Laboratory at the University of Otago, New Zealand.

The excited-state lifetimes of the emissions were determined from samples irradiated using a LaserScience VSL 337 laser; 123 time-resolved emission decays were measured (through an appropriate band-pass filter) on an EMI-Gencom RFI/216F detector connected to a Tektronix TDS620A oscilloscope. The average of these data was digitized and analyzed using the computer program KaleidaGraph (Synergy Software)[14] on which curve fitting was carried out. One or more exponential curves were fitted to the measured emission decays; fits having $R > 0.99$ and an even distribution of the residuals about a mean ($\chi^2 \leq 5 \times 10^{-5}$) were accepted as authentic.

Theoretical Calculations. Theoretical calculations were performed on $[Au(\mathbf{1})_2]^+$ and $[Au(\mathbf{4})_2]^+$ ($\mathbf{4}$ = 1,2-bis(dimethylphosphino)ethane) using the ADF program[15] (2000 version) on Linux-based Pentium III 600 MHz computers. For the geometry optimizations, triple-ζ basis sets (Type IV) were used for the Au atoms and double-ζ basis sets with polarization functions (Type III) for P, C, and H atoms. Orbitals up to and including 4f(Au), 2p(P), and 1s(C) were treated using the frozen core approximation. All calculations employed the local density approximation to the exchange potential and the correlation potential of Vosko, Wilk, and Nusair.[16] The gradient corrections of Becke[17] and Perdew[18] were also included, along with scalar relativistic corrections using the ZORA formalism.[19] Geometries were optimized using the gradient algorithm of Versluis and Ziegler.[20] To reduce the computational effort, geometries for both $[Au(\mathbf{1})_2]^+$ and $[Au(\mathbf{4})_2]^+$ were optimized within the constraints of D_2 symmetry. For $[Au(\mathbf{1})_2]^+$, the C−C and C−H distances associated with the phenyl rings were fixed at 1.40 and 1.09 Å, respectively, these values being obtained from a separate optimization of C_6H_6. Both singlet and triplet excitation energies were calculated using the time-dependent DFT functionality available in the ADF program. The calculations were undertaken on the optimized geometries employing the same basis sets and methods used above.

Table 1. Crystallographic Data and Experimental Parameters for $(\pm)$-$[Au_2\{(R^*,R^*)\text{-}\mathbf{2}\}_2](PF_6)_2 \cdot 2.77CH_2Cl_2 \cdot H_2O$

mol formula	$C_{84}H_{84}Au_2P_8(PF_6)_2 \cdot (CH_2Cl_2)_{2.77} \cdot H_2O$
fw, g mol^{-1}	2278.52
cryst syst	triclinic
space group	$P\bar{1}$
cryst color	colorless
cell dimension	
a, Å	14.8211(2)
b, Å	14.9246(2)
c, Å	23.7197(3)
α, deg	73.777(1)
β, deg	81.865(1)
γ, deg	87.654(1)
V, Å^3	4987.15(12)
Z	2
d_{calcd}, mg m^{-3}	1.517
cryst dimension, mm	0.37 × 0.25 × 0.06
instrument	Enraf-Nonius Kappa CCD diffractometer
X-radiation	Mo Kα
λ, Å	0.71073
μ, mm^{-1}	3.31
T, K	200
unique reflns	22668
obsd reflns	12603 [$I > 3\sigma(I)$]
data range, deg in θ	3−27
R	0.0376
wR	0.0413

[*T*-4-[(*R,*R**)]]-(±)-Bis(1,1,4,7,10,10-hexaphenyl-1,4,7,10-tetraphosphadecane)digold(I) Hexafluorophosphate, (±)-[Au_2-{(*R**,*R**)-**2**}$_2$](PF$_6$)$_2$.** (*R**,*R**)-(±)-**2** (1.00 g, 1.49 mmol) was dissolved in dichloromethane (20 mL), and Me_2SAuCl (0.44 g, 1.49 mmol) was added. The colorless solution was stirred for 0.5 h before addition of NH_4PF_6 (2.16 g, 13.30 mmol) in water (30 mL). The two-phase mixture was stirred at room temperature for 2 h. The organic layer was separated, dried over magnesium sulfate, and the solvent removed, leaving a colorless powder. Recrystallization of this material from dichloromethane/diethyl ether gave a crystalline colorless solid, mp >230 °C. Yield: 1.31 g (87%). Anal. Calcd for $C_{84}H_{84}Au_2F_{12}P_{10}$: C, 49.8; H, 4.2. Found: C, 49.6; H, 4.0. $^{31}P\{^1H\}$ NMR ($CDCl_3$): δ 23.3−25.0 (overlapping multiplets, 4P, outer phosphorus), 17.5−19.2 (overlapping multiplets, 4P, inner phosphorus), −143.9 (sept, 1P, $^1J_{PF}$ = 709.1 Hz, PF_6^-). ^1H NMR (CD_2Cl_2): 2.10 (b, ca. 4H, C−H), 2.40 (b, ca. 2H, C−H), 2.63 (b, ca. 6H, C−H), 6.95−7.45 (overlapping multiplets, 30 H, Ar−H). ^{13}C NMR (δ, CD_2Cl_2): 26.80, 27.53, 30.89, 129.03, 129.10, 129.16, 124.499, 129.56, 130.82, 130.95, 131.11, 131.35, 132.38, 132.48, 132.58, 132.72, 133.05. MS *m*/*z*: 2023.5 $[M]^+$ (2%), 1879.1 (4%) $[M^+ - PF_6]$, 1734.1 (2%), $[M^+ - 2PF_6]$, 1385.0, 1062.9, 867.0 (100%)[0.5 $M^+ - PF_6$]. The sample for crystallography was obtained by allowing a 2:1 dichloromethane/diethyl ether solution of the complex to slowly evaporate in the atmosphere.

Structural Analysis. Crystal data for $(\pm)$-$[Au_2\{(R^*,R^*)\text{-}\mathbf{2}\}_2](PF_6)_2 \cdot 2.77CH_2Cl_2 \cdot H_2O$ are summarized in Table 1. Important bond

(10) Airey, A. L.; Cook, V. C.; Swiegers, G. F.; Willis, A. C.; Zank, H.; Wild, S. B., in preparation.
(11) (a) Berners-Price, S. J.; Mazid, M. A.; Sadler, P. J. *J. Chem. Soc., Dalton Trans.* **1984**, 969. (b) Bates, P. A.; Waters, J. M. *Inorg. Chim. Acta* **1984**, *81*, 151. (c) Harker, C. S. W.; Tiekink, E. R. T.; Whitehouse, M. W. *Inorg. Chim. Acta* **1991**, *181*, 23.
(12) McArdle, J. V.; Brossard, G. E. *J. Chem. Soc., Dalton Trans.* **1990**, 2219.
(13) Webb, K. S.; Dunn, A. B.; Wang, H. H.; Williams, J. M. *Inorg. Synth.* **1992**, *29*, 47.
(14) *KaleidaGraph*, version 3.5; Synergy Software: Reading, PA, 1986−2000.
(15) Baerends, E. J.; Bérces, A.; Bo, C.; Boerrigter, P. M.; Cavallo, L.; Deng, L.; Dickson, R. M.; Ellis, D. E.; Fan, L.; Fischer, T. H.; Fonseca Guerra, C.; van Gisbergen, S. J. A.; Groeneveld, J. A.; Gritsenko, O. V.; Harris, F. E.; van den Hoek, P.; Jacobsen, H.; van Kessel, G.; Kootstra, F.; van Lenthe, E.; Osinga, V. P.; Philipsen, P. H. T.; Post, D.; Pye, C.; Ravenek, W.; Ros, P.; Schipper, P. R. T.; Schreckenbach, G.; Snijders, J. G.; Sola, M.; Swerhone, D.; te Velde, G.; Vernooijs, P.; Versluis, L.; Visser, O.; van Wezenbeek, E.; Wiesenekker, G.; Wolff, S. K.; Woo, T. K.; Ziegler, T. ADF; Amsterdam, The Netherlands, 2000.
(16) Vosko, S. H.; Wilk, L.; Nusair, M. *Can. J. Phys.* **1980**, *58*, 1200.
(17) Becke, A. D. *Phys. Rev. A: At., Mol., Opt. Phys.* **1988**, *38*, 3098.
(18) Perdew, J. P. *Phys. Rev. B* **1986**, *33*, 8822.
(19) van Lenthe, E.; Ehlers, A. E.; Baerends, E. J. *J. Chem. Phys.* **1999**, *110*, 8943.
(20) Versluis, L.; Ziegler, T. J. *J. Chem. Phys.* **1988**, *88*, 322.

Table 2. Selected Bond Distances and Angles for $[Au_2\{(R,R)\text{-}\mathbf{2}\}_2]^{2+}$ in the Unit Cells of (±)-$[Au_2\{(R^*,R^*)\text{-}\mathbf{2}\}_2](PF_6)_2\cdot 2.77CH_2Cl_2\cdot H_2O$ (Figures 6 and 7a) and (−)-$[Au_2\{(R,R)\text{-}\mathbf{2}\}_2](PF_6)_2$ (Figure 7b)[a]

	(±)-$[Au_2\{(R^*,R^*)\text{-}\mathbf{2}\}_2](PF_6)_2\cdot 77CH_2Cl_2\cdot H_2O$	(−)-$[Au_2\{(R,R)\text{-}\mathbf{2}\}_2](PF_6)_2$[a]
	Bond Distances (Å)	
Au(1)−P(11)	2.4129(16)	2.406(4)
Au(1)−P(12)	2.3975(16)	2.394(4)
Au(1)−P(21)	2.4160(16)	2.419(4)
Au(1)−P(22)	2.4001(16)	2.379(4)
Au(2)−P(13)	2.3936(15)	2.417(4)
Au(2)−P(14)	2.3953(16)	2.421(4)
Au(2)−P(23)	2.3878(15)	2.394(4)
Au(2)−P(24)	2.4057(16)	2.447(4)
Au(1)−Au(2)	6.2094(3)	6.2144(2)
	Bond Angles (deg)	
P(11)−Au(1)−P(12)	86.34(6)	85.7(1)
P(11)−Au(1)−P(21)	117.88(5)	119.8(1)
P(11)−Au(1)−P(22)	127.26(6)	124.1(1)
P(12)−Au(1)−P(21)	126.48(6)	124.9(1)
P(12)−Au(1)−P(22)	118.56(5)	120.99(1)
P(21)−Au(1)−P(22)	85.29(6)	86.0(1)
P(13)−Au(2)−P(14)	85.90(5)	86.1(1)
P(13)−Au(2)−P(23)	121.20(5)	115.0(0)
P(13)−Au(2)−P(24)	120.08(6)	128.5(1)
P(14)−Au(2)−P(23)	127.96(6)	132.8(1)
P(14)−Au(2)−P(24)	118.88(5)	115.4(1)
P(23)−Au(2)−P(24)	86.92(6)	85.0(1)

[a] Data taken from ref 5.

lengths and angles are listed in Table 2. Full details of the structural analysis are provided as Supplementary Material. The crystals were extracted from the dichloromethane/diethyl ether solution with a Pasteur pipet and deposited directly into perfluoropolyether oil. A crystal was quickly selected, mounted on a cryoloop, and transferred to the diffractometer where it was cooled immediately under a stream of N_2 at 200 K. The crystallographic asymmetric unit contains one $[Au_2(C_{42}H_{42}P_4)_2]^{2+}$ ion, two PF_6^- ions, dichloromethane molecules of solvation at four sites, and a water molecule disordered over two sites. The unit cell contains two nonsuperimposable asymmetric units, i.e., two mirror image $[Au_2(C_{42}H_{42}P_4)_2]^{2+}$ ions. Displacement parameters of the fluorine atoms in one of the PF_6^- ions in the asymmetric unit showed considerable anisotropy of their displacement parameters. An equatorial ring of electron density centered on P(40), with an appropriate radius and orientation, was added to the model, and F(46) was divided over two sites. Solvate molecules occupy channels running in the *c* direction through the unit cell. Difference electron-density maps clearly show dichloromethane molecules at four locations, but their displacement parameters became very large when refined with full occupancies. Consequently, the occupancies of each molecule were allowed to refine, with the isotropic displacement parameters of the individual atoms being initially fixed at appropriate values, but later being refined also. Weak restraints were imposed on distances and angles within these molecules. Final occupancies for the dichloromethane sites were 0.70(1), 0.85(1), 0.60(1), and 0.62(2). A further two peaks were observed that appeared to be sites for water molecules with a combined occupancy of 1. Hydrogen atoms attached to carbon atoms were included at idealized positions and ride on the atoms to which they are bonded. Hydrogen atoms for the water molecules were not included.

Results and Discussion

Digold(I) Complexes. The $^{31}P\{^1H\}$ NMR spectrum of the digold(I) complex of the racemic diastereomer of tetraphos, (±)-$[Au_2\{(R^*,R^*)\text{-}\mathbf{2}\}_2](PF_6)_2$, indicates that it exists in solution as the racemate, viz. (+)-$[Au_2\{(S,S)\text{-}\mathbf{2}\}_2](PF_6)_2$ and (−)-$[Au_2\{(R,R)\text{-}\mathbf{2}\}_2](PF_6)_2$ (Figure 1).[5,21] The complex of the meso diastereomer of the ligand, $[Au_2\{(R^*,S^*)\text{-}\mathbf{2}\}_2](PF_6)_2$, is a head-to-head helicate in which the two chiral metal stereocenters have opposite configurations.[5c,8,10]

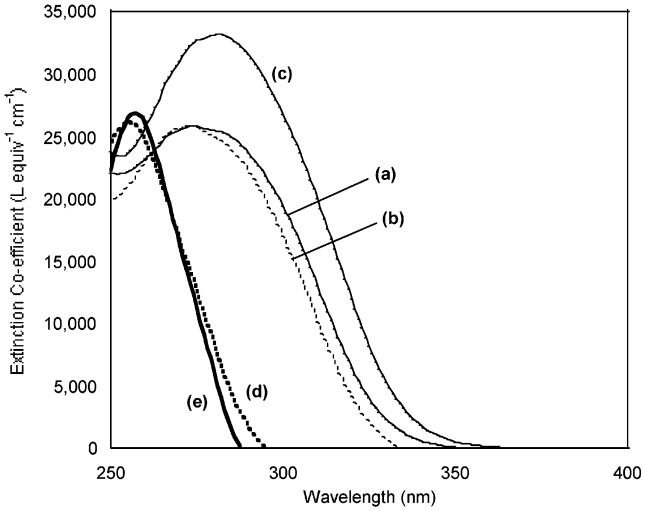

Figure 2. UV−visible spectra in dichloromethane of (a) (±)-$[Au_2\{(R^*,R^*)\text{-}\mathbf{2}\}_2](PF_6)_2$, (b) $[Au_2\{(R^*,S^*)\text{-}\mathbf{2}\}_2](PF_6)_2$, (c) $[Au(\mathbf{1})_2]PF_6$, (d) (*R**,*S**)-**2**, and (e) (*R**,*R**)-(±)-**2**.

Electronic Absorption Spectra. Each of the digold(I) complexes displays a broad UV absorption band centered at 277 nm in dichloromethane (Figure 2). The free ligands, (*R**,*R**)-(±)-**2** and (*R**,*S**)-**2**, absorb similarly with maxima at 254−258 nm (Figure 2). The resemblance of the metal complex and free ligand absorptions suggests significant $\pi \rightarrow \pi^*$ (Ph) character in the transitions.[22]

(21) The coordination of the phosphine to the metal is stereospecific with retention of configuration at phosphorus: the apparent inversion that occurs when (*S*,*S*)-(+)-**2** forms (−)-$[Au_2\{(R,R)\text{-}\mathbf{2}\}_2](PF_6)_2$ is a consequence of the Cahn−Ingold−Prelog (CIP) rules for assigning absolute configurations. See: Cahn, R. S.; Ingold, C. K.; Prelog, V. *Angew. Chem., Int. Ed. Engl.* **1966**, *5*, 385.

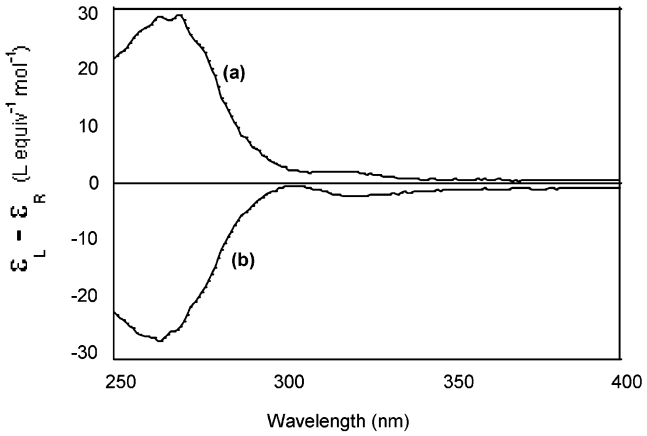

Figure 3. Circular dichroism spectra at 293 K in dichloromethane of (a) (−)-$[Au_2\{(R,R)\text{-}\mathbf{2}\}_2](PF_6)_2$ and (b) (+)-$[Au_2\{(S,S)\text{-}\mathbf{2}\}_2](PF_6)_2$.

The absorption bands for the metal complexes broaden and develop distinct shoulders tailing off almost into the visible when the spectra are recorded in ethanol. Solvatochromic shifts of this type are characteristic of MLCT absorptions; in dichloromethane, these bands are obscured by the large $\pi-\pi^*$ (Ph) bands.[23] The corresponding disilver(I) complexes $[Ag_2\{(R^*,R^*)$- and $(R^*,S^*)\text{-}\mathbf{2}\}_2](PF_6)_2$ display similar absorptions, with maxima at 264 nm. These are consistent with the presence of MLCT absorptions, because Au(I) is more readily reduced than Ag(I).[23] Further data consistent with MLCT bands were found in the circular dichroism spectra of the individual enantiomers (−)-$[Au_2\{(R,R)\text{-}\mathbf{2}\}_2](PF_6)_2$ and (+)-$[Au_2\{(S,S)\text{-}\mathbf{2}\}_2](PF_6)_2$, which contain small but distinct dichroic bands at 305−340 nm, well separated from the major band at 268 nm (Figure 3).

Luminescence in Solution. Solutions of the digold(I) helicates in the concentration range 0.002−0.5 M are nonemissive when irradiated at 277 nm under oxygen-free conditions in a variety of solvents, including dichloromethane. Above 0.5 M, only very weak emissions at λ_{max} 435 nm were detected by fluorescence spectroscopy.

Luminescence in the Solid State. Crystalline samples of the digold(I) complexes are intensely luminescent with broad emission profiles being centered at λ_{max} 580 nm (Figure 4a) and 620 nm (Figure 5a). The Stokes shifts for these emissions are substantial, viz. 303 and 343 nm for the complexes of the racemic and meso ligands, respectively. These shifts are of the same order of magnitude as those observed for $[Au(\mathbf{3a},\mathbf{b})_2]PF_6$ (340−400 nm).[2]

The digold(I) complexes display single-exponential excited-state lifetimes in the crystalline state. These are, however, different for (±)-$[Au_2\{(R^*,R^*)\text{-}\mathbf{2}\}_2](PF_6)_2$ (τ 9.4 μs) and the individual enantiomers (−)-$[Au_2\{(R,R)\text{-}\mathbf{2}\}_2](PF_6)_2$ and (+)-$[Au_2\{(S,S)\text{-}\mathbf{2}\}_2](PF_6)_2$ (τ 8.6 μs). If the racemate consists of an equal mixture of the two enantiomers, its emission may reasonably have been expected to be identical to those of the individual enantiomers. Crystals of $[Au_2\{(R^*,S^*)\text{-}\mathbf{2}\}_2](PF_6)_2$ display an excited-state lifetime of 5.3 μs.

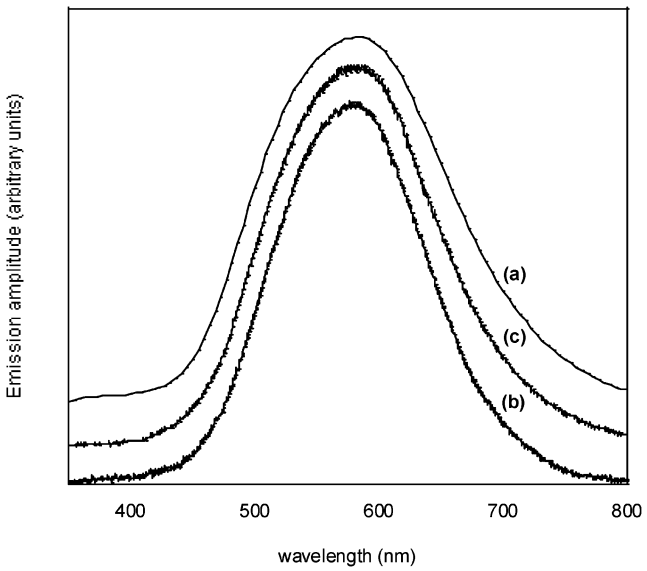

Figure 4. Normalized emission spectra of (±)-$[Au_2\{(R^*,R^*)\text{-}\mathbf{2}\}_2](PF_6)_2$ as (a) a crystalline solid at 293 K, (b) an amorphous solid at 293 K prepared by evaporation of a dichloromethane solution, and (c) a dispersion (0.005 g/g PMMA) within a cast film of PMMA at 293 K.

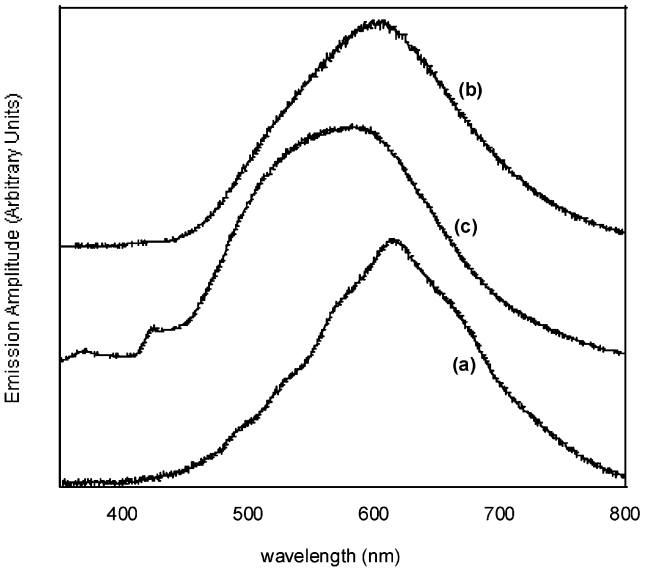

Figure 5. Normalized emission spectra of $[Au_2\{(R^*,S^*)\text{-}\mathbf{2}\}_2](PF_6)_2$ as (a) a crystalline solid at 293 K, (b) an amorphous solid at 293 K prepared by evaporation of a dichloromethane solution, and (c) a dispersion (0.005 g/g PMMA) within a cast film of PMMA at 293 K.

To assist in the rationalization of these results, we reexamined the previously published X-ray crystal structure of (−)-$[Au_2\{(R,R)\text{-}\mathbf{2}\}_2](PF_6)_2$[5] and carried out an X-ray structure determination on (±)-$[Au_2\{(R^*,R^*)\text{-}\mathbf{2}\}_2](PF_6)_2\cdot 2.77CH_2Cl_2\cdot H_2O$. The latter complex was isolated as a colorless, crystalline, mixed solvate that rapidly lost solvent upon exposure to the air. Luminescence studies were conducted on analytically pure, solvent-free microcrystals for which an X-ray crystal structure could not be obtained. The solvated crystals were, however, isolated in perfluorinated polyether oil and successfully subjected to an X-ray diffraction study. The centrosymmetric unit cell of (±)-[Au_2-

(22) Silverstein, R. M.; Bassler, G. C.; Morrill, T. C. *Spectrometric Identification of Organic Compounds*, 5th ed.; John Wiley & Sons: New York, 1991; p 306.
(23) Lever, A. B. P. *Inorganic Electronic Spectroscopy*, 2nd ed.; Elsevier: Amsterdam, The Netherlands, 1984; p 208.

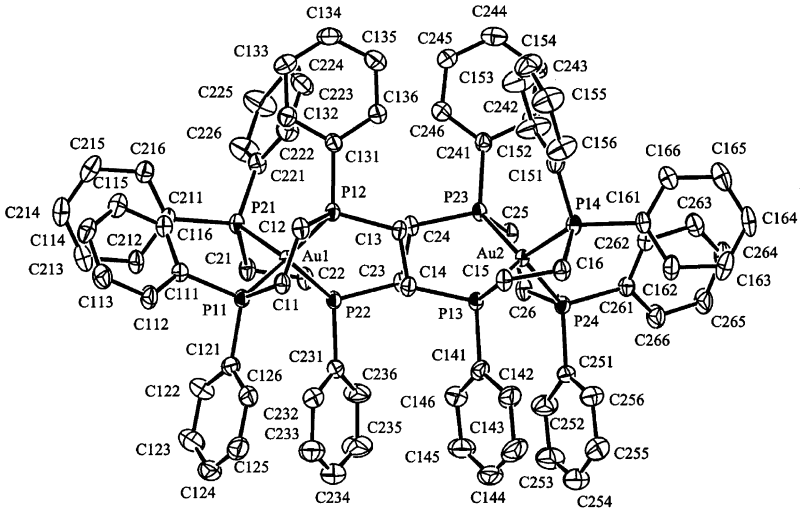

Figure 6. Thermal ellipsoid diagram of $[Au_2\{(R,R)\text{-}\mathbf{2}\}_2]^{2+}$ in the unit cell of $(\pm)\text{-}[Au_2\{(R^*,R^*)\text{-}\mathbf{2}\}_2](PF_6)_2{\cdot}2.77CH_2Cl_2{\cdot}H_2O$ with labeling of selected atoms. Ellipsoids show 30% probability levels. Hydrogen atoms have been deleted for clarity.

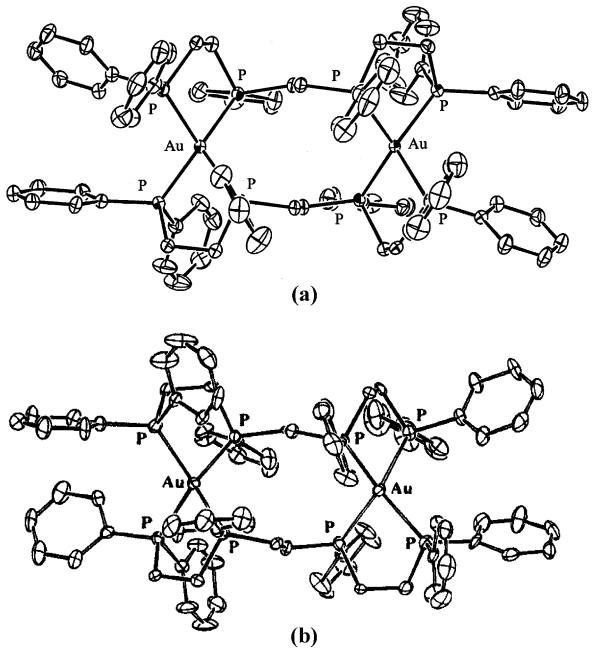

Figure 7. Thermal ellipsoid diagrams with labeling of selected atoms of $[Au_2\{(R,R)\text{-}\mathbf{2}\}_2]^{2+}$ in the unit cell of (a) $(\pm)\text{-}[Au_2\{(R^*,R^*)\text{-}\mathbf{2}\}_2](PF_6)_2{\cdot}2.77CH_2Cl_2{\cdot}H_2O$ and (b) $(-)\text{-}[Au_2\{(R,R)\text{-}\mathbf{2}\}_2](PF_6)_2$.[5] Ellipsoids contain 30% probability levels. Hydrogen atoms have been deleted for clarity.

$\{(R^*,R^*)\text{-}\mathbf{2}\}_2](PF_6)_2{\cdot}2.77CH_2Cl_2{\cdot}H_2O$ contains both enantiomers of the cation and associated anions and solvent molecules. The complex therefore crystallizes as a racemate and not as a conglomerate of crystals of the individual molecules. The thermal elipsoid diagram for the $[Au_2\{(R,R)\text{-}\mathbf{2}\}_2]^+$ ion within the racemate is shown in Figure 6.

Figure 7 shows the structures of the $[Au_2\{(R,R)\text{-}\mathbf{2}\}_2]^{2+}$ ion in $(\pm)\text{-}[Au_2\{(R^*,R^*)\text{-}\mathbf{2}\}_2](PF_6)_2{\cdot}2.77CH_2Cl_2{\cdot}H_2O$ and in $(-)\text{-}[Au_2\{(R,R)\text{-}\mathbf{2}\}_2](PF_6)_2$.[5] The molecular structure of the $[Au_2\{(R,R)\text{-}\mathbf{2}\}_2]^{2+}$ ion is essentially identical in the two unit cells: both have parallel helical conformations (Figure 1a) and comparable bond lengths and angles in the central 10-membered ring containing the two metal ions (Table 2). The peripheral five-membered rings, however, have different conformations: $\delta,\lambda,\delta,\lambda$ in $(\pm)\text{-}[Au_2\{(R^*,R^*)\text{-}\mathbf{2}\}_2](PF_6)_2{\cdot}2.77CH_2Cl_2{\cdot}H_2O$ and $\delta,\delta,\delta,\lambda$ in $(-)\text{-}[Au_2\{(R,R)\text{-}\mathbf{2}\}_2](PF_6)_2$. The two structures therefore differ only in the orientation and pairing of the individual *P*-phenyl groups. It is unlikely that the solid-state structure of the cation in $(\pm)\text{-}[Au_2\{(R^*,R^*)\text{-}\mathbf{2}\}_2](PF_6)_2{\cdot}2.77CH_2Cl_2{\cdot}H_2O$ would change substantially during loss of solvent (to become identical with that of the enantiomerically pure cation in $(-)\text{-}[Au_2\{(R,R)\text{-}\mathbf{2}\}_2](PF_6)_2$). The luminescence lifetime of $[Au_2\{(R,R)\text{-}\mathbf{2}\}_2]^{2+}$ is therefore attributable to the differences in the phenyl-pairing interactions in $(\pm)\text{-}[Au_2\{(R^*,R^*)\text{-}\mathbf{2}\}_2](PF_6)_2{\cdot}2.77CH_2Cl_2{\cdot}H_2O$ and in $(-)\text{-}[Au_2\{(R,R)\text{-}\mathbf{2}\}_2](PF_6)$ in the solid state. As noted in our previous work[5] and elsewhere,[24] concerted inter- and intramolecular edge-to-face and face-to-face interactions between phenyl groups play a significant role in the crystal lattices of metal complexes containing phosphorus−phenyl ligands. Changes in these interactions may induce significant alterations in the solid-state packing and thereby influence physical properties.[5]

To test this deduction, crystals of the racemic complex and the corresponding enantiomers were separately dissolved in dichloromethane and acetonitrile, and the solutions were evaporated to produce amorphous solids and glasses. New inter- and intramolecular phenyl pairings would have been created in this process. The resulting materials exhibited new, reproducible, biexponential decays that were indeed different from those of the crystalline samples (Table 3). The steady-state emission profiles of the complexes were not substantially changed, however (Figures 4b and 5b). The excitation spectra of all of the above complexes, both crystalline and amorphous, monitored at their respective emission maxima, closely matched the UV−visible spectra of the digold(I) complexes.

Luminescence in Poly(methyl methacrylate). To establish the influence of intermolecular phenyl pairings relative to their intramolecular analogues, the digold(I) complexes were dispersed within cast films of PMMA at a variety of concentrations (0.0005−0.1 g complex/g polymer). Increasing the dispersion of the digold(I) complexes was expected

(24) Dance, I.; Scudder, M. *J. Chem. Soc., Chem. Commun*. **1995**, 1039.

Table 3. Emissive Properties at 293 K of (±)-$[Au_2\{(R^*,R^*)\text{-}\mathbf{2}\}_2](PF_6)_2$, $[Au_2\{(R^*,S^*)\text{-}\mathbf{2}\}_2](PF_6)_2$, and $[Au(\mathbf{1})_2]PF_6$

compound	emission data	
	λ_{max} (nm)	τ (μs)[a]
(±)-$[Au_2\{(R^*,R^*)\text{-}\mathbf{2}\}_2](PF_6)_2$		
crystalline solid	585	9.4
amorphous solid (from CH_2Cl_2)	585	5.3, 0.5[b]
amorphous solid (from CH_3CN)	575	5.1, 0.7[b]
in PMMA (0.005 g/g PMMA)	580	5.8, 1.3[b]
$[Au_2\{(R^*,S^*)\text{-}\mathbf{2}\}_2](PF_6)_2$		
crystalline solid	615	5.3
amorphous solid (from CH_2Cl_2)	600	5.3, 0.4[b]
amorphous solid (from CH_3CN)	595	5.1, 1.0[b]
in PMMA (0.005 g/g PMMA)	590	5.1, 1.1[b]
$[Au(\mathbf{1})_2]PF_6$		
crystalline solid	595	4.5
amorphous solid (from CH_2Cl_2)	595	4.1, 0.7[b]
amorphous solid (from CH_3CN)	595	1.7
in PMMA (0.005 g/g PMMA)	595	5.4, 0.9[b]

[a] Data collected at 600 nm. [b] Double exponential.

to favor the formation of intramolecular phenyl over intermolecular pairings. The steady-state emission profiles of the films were similar to those obtained for the corresponding solids (Figures 4c and 5c). For each form of the digold(I) complexes, the excited-state lifetimes of the film samples were identical and unaffected by concentration, although they differed from those observed previously, including those of the amorphous solids and glasses. Significantly, the excited-state lifetimes of the separated enantiomers in PMMA matched those of the *racemic* complex, indicating that their molecular structures in this medium were identical and demonstrating that aggregation had not occurred within the films. The excitation spectra of the films matched the UV−visible spectra of the digold(I) complexes. The emissions of the complexes in PMMA are therefore unequivocally molecular and most likely associated with a new set of exclusively intramolecular phenyl−phenyl interactions within the isolated species.

Luminescence of $[Au(\mathbf{1})_2]PF_6$. To determine whether gold−gold interactions or the presence of particular conformers of the complex played roles in the luminescence properties of the digold(I) complexes, the related mononuclear complex $[Au(\mathbf{1})_2]PF_6$ was investigated.[11] As for the digold(I) complexes, $[Au(\mathbf{1})_2]PF_6$ exhibits a major absorption band at λ_{max} 282 nm (Figure 2),[12] and the X-ray crystal structure of $[Au(\mathbf{1})_2]SbF_6\cdot$MeOH contains pronounced phenyl−phenyl interactions.[11a]

Crystalline $[Au(\mathbf{1})_2]PF_6$ exhibits luminescence properties almost identical to those of the digold(I) helicates, being nonemissive in solution but strongly emissive in the solid state and having steady-state emission profiles in the crystalline and amorphous solid states that are very similar to the emissions for the digold(I) complexes (Figure 8a,b). The excited-state lifetimes for the crystalline and various amorphous solid states of the complex are also similar to those of the digold(I) complexes (Table 3). Cast films of PMMA containing $[Au(\mathbf{1})_2]PF_6$ display identical emissive properties over the concentration range of 0.0005−0.1 g/g PMMA, and their emissions closely match those of the digold(I) complexes under otherwise identical circumstances (Figure 8c).

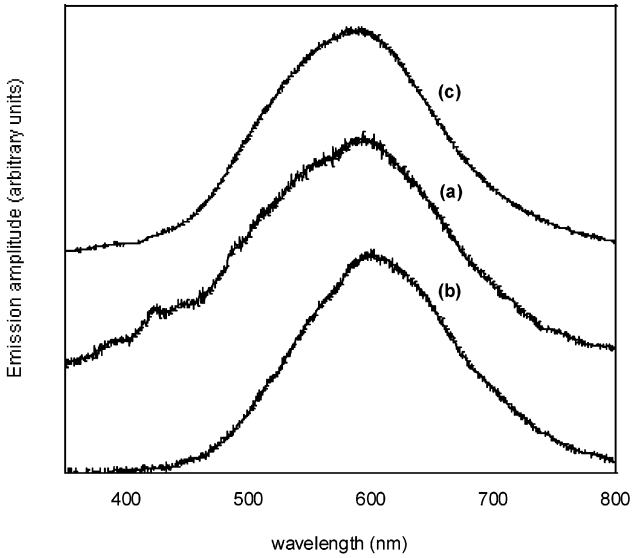

Figure 8. Normalized emission spectra of $[Au(\mathbf{1})_2]PF_6$ as (a) a crystalline solid at 293 K, (b) an amorphous solid at 293 K prepared by evaporation of a dichloromethane solution, and (c) a dispersion (0.005 g/g PMMA) within a cast film of PMMA at 293 K.

Table 4. Selected Geometric Parameters for $[Au(\mathbf{1})_2]^+$ and $[Au(\mathbf{4})_2]^+$ in the Ground State

	$[Au(\mathbf{1})_2]^+$		$[Au(\mathbf{4})_2]^+$
	exptl	calcd	calcd
Au−P / Å	2.40[a]	2.46	2.52
P(1)−Au−P(2) / deg	86.5[a]	84.7	86.8
P(1)−Au−P(3) / deg	115[a]	114	118
P(1)−Au−P(4) / deg	128[a]	133	126
P−C_s[b] / Å	1.82[a]	1.84[a]	1.91[a]
P−C_b[c] / Å	1.85[a]	1.89	1.94

[a] Averaged value. [b] C_s carbon in either phenyl or methyl substituents. [c] C_b carbon in ethylene bridge.

The mechanisms of emission in the gold(I) complexes of **1** and (*R**,*R**)-(±)/(*R**,*S**)-**2** appear to be identical. The presence of two Au(I) ions in a complex does not influence the luminescence, nor is the luminescence limited to a particular conformer because the digold(I) cations consist of two mononuclear components that are structurally similar to $[Au(\mathbf{1})_2]PF_6$.

Theoretical Calculations. Theoretical computations of the expected transitions were carried out for $[Au(\mathbf{1})_2]^+$ and its methylated analogue $[Au(\mathbf{4})_2]^+$ (**4** = 1,2-bis(dimethylphosphino)ethane) using DFT. The latter complex served as a simplified model of $[Au(\mathbf{3c})_2]^+$.

Optimized values for selected geometric parameters are given in Table 4 together with the reported crystallographic values for $[Au(\mathbf{1})_2]Cl\cdot 2H_2O$.[11b] In general, good agreement exists between the calculated and experimental structures for $[Au(\mathbf{1})_2]^+$, particularly in relation to the P−Au−P bond angles. The calculated Au−P and P−C distances in the cations are approximately 0.02−0.05 Å longer than those observed. The calculated P−Au−P angles for $[Au(\mathbf{4})_2]^+$ are similar to those obtained for $[Au(\mathbf{2})_2]^+$, but the Au−P distances are ca. 0.05 Å longer. The optimized structure for $[Au(\mathbf{1})_2]^+$ exhibits prominent stacking of the phenyl rings on opposite 1,2-ethano bridges with inter-ring separations of 3.5 Å (Figure 9).

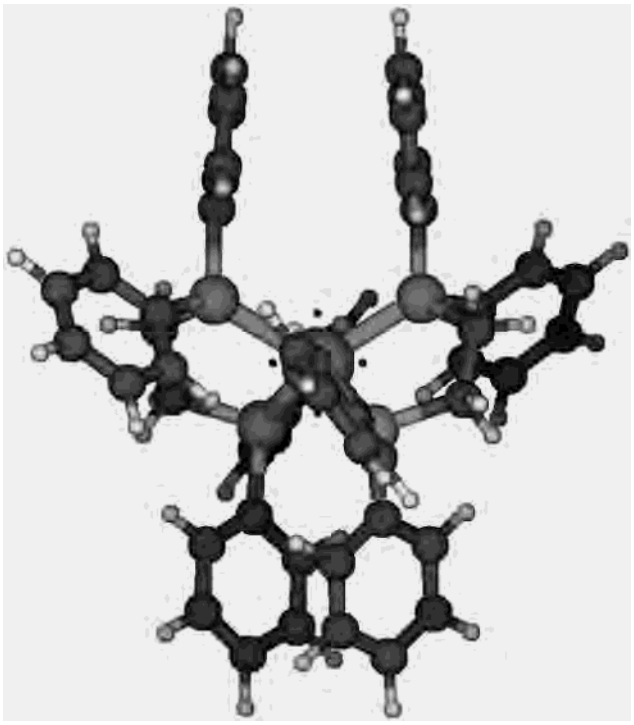

Figure 9. Optimized ground-state structure of isolated $[Au(\mathbf{1})_2]^+$ as calculated using density functional theory. The phenyl rings on opposite ethylene bridges display prominent stacking with inter-ring separations of 3.5 Å.

Table 5. Calculated Absorption Energies and Intensities for $[Au(\mathbf{1})_2]^+$

Energy/nm			
calcd	obsd	oscillator strength (calcd)	description
		Singlet Transitions	
288		0.17	$\pi \rightarrow \pi^*$
295	282	0.07	$\pi \rightarrow \pi^*$
311		0.21	MLCT/$\pi \rightarrow \pi^*$
		Triplet Transitions	
394	415	not calcd	MLCT
400		not calcd	MLCT
426	541	not calcd	MLCT
427		not calcd	MLCT

The calculated singlet and triplet absorption energies and intensities for the most intense lower-lying singlet excitations (oscillator strength > 0.05) in $[Au(\mathbf{1})_2]^+$ are given in Table 5. The calculations indicate a HOMO−LUMO gap of ca. 2.9 eV with the $36B_1$ HOMO comprising mainly Au(d_{xy}) and P(p) orbitals and the pseudodegenerate LUMO levels ($38B_2$, 39A) being essentially π^* orbitals associated with the phenyl rings. The major absorption band for $[Au(\mathbf{1})_2]^+$ at λ_{max} 282 nm was best assigned to phenyl $\pi \rightarrow$ p* transitions on the basis of the calculated transitions at 285−331 nm. A number of weaker singlet transitions were calculated down to 417 nm, which explains the weaker tail extending into the visible region in the absorption spectrum of the complex. On the basis of these calculations, the lower-lying singlet transitions have significant MLCT character. The lowest-lying triplet transitions lie between 392 and 425 nm as predominantly Au(d)−P(p) → p* MLCT transitions.

Calculations on $[Au(\mathbf{4})_2]^+$ indicated no singlet or triplet excitations below 308 nm. This result is consistent with the observed nonemissive nature of the *P*-cyclohexyl-substituted phosphine complex $[Au(\mathbf{3c})_2]PF_6$.

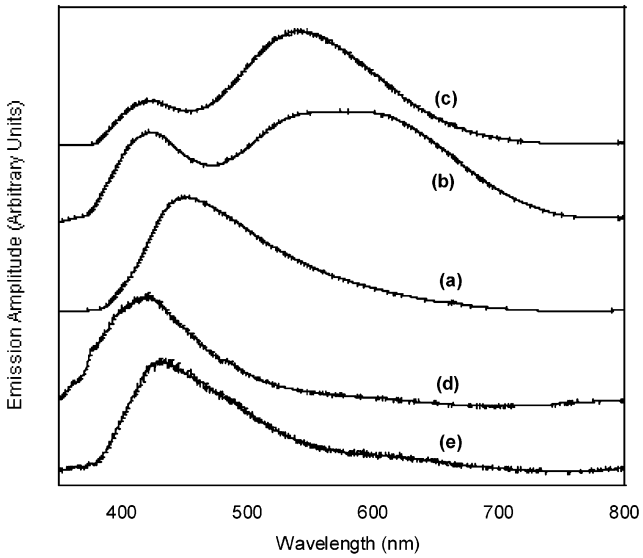

Figure 10. Normalized emission spectra as an ethanol glass at 77 K of (a) (±)-$[Au_2\{(R^*,R^*)\text{-}\mathbf{2}\}_2](PF_6)_2$, (b) $[Au_2\{(R^*,S^*)\text{-}\mathbf{2}\}_2](PF_6)_2$, (c) $[Au(\mathbf{1})_2]PF_6$, (d) $[Ag_2\{(R^*,S^*)\text{-}\mathbf{2}\}_2](PF_6)_2$, and (e) (±)-$[Ag_2\{(R^*,R^*)\text{-}\mathbf{2}\}_2](PF_6)_2$.

Emissions at 77 K. To determine whether $[Au(\mathbf{1})_2]PF_6$ and $[Au_2\{(R^*,R^*)/(R^*,S^*)\text{-}\mathbf{2}\}_2](PF_6)_2$ emit at the calculated wavelengths of 392−425 nm at low temperature, samples of the complexes were dissolved in degassed ethanol (<0.0005 M), and the solutions were frozen at 77 K under inert atmosphere. Glasses of $[Au(\mathbf{1})_2]PF_6$ and $[Au_2\{(R^*,S^*)\text{-}\mathbf{2}\}_2](PF_6)_2$ exhibited minor emission bands at λ_{max} 415 nm and major emission bands at λ_{max} 520−595 nm (Figure 10b,c). The emission of (±)-$[Au_2\{(R^*,R^*)\text{-}\mathbf{2}\}_2](PF_6)_2$ under these conditions was superficially monomodal with λ_{max} 450 nm (Figure 10a); time-resolved decay measurements indicated, however, two distinct emission bands at ca. λ_{max} 420 nm and λ_{max} 520 nm. Emissions for the individual enantiomers of $[Au_2\{(R^*,R^*)\text{-}\mathbf{2}\}_2](PF_6)_2$ were identical to that of the racemate. The excitation spectra of the glasses, monitored at both the high- and low-energy emission maxima, matched the UV−visible spectra of the corresponding complexes, although the latter were red-shifted by ca. 5 nm in each case.

Lifetime measurements indicated that the emissions at λ_{max} 415−450 nm were unusually long-lived (τ ca. 192−309 μs). Consistent lifetimes could not be calculated for the digold(I) complexes because of the weakness of the band, but the emission was stronger for $[Au(\mathbf{1})_2]PF_6$, which displayed lifetimes of τ 251.0 ± 20.5 μs (λ_{max} 415 nm) and τ 14.9 ± 4.6 μs (λ_{max} 541 nm) ($R = 0.992$; $\chi^2 = 5.3 \times 10^{-6}$ over four samples examined). Luminescence anisotropy measurements confirmed the presence of two differently oriented emissions for each of the compounds examined (Figure 11).

Summary

Two emissive relaxation mechanisms exist for $[Au(\mathbf{1})_2]PF_6$ and $[Au_2(\mathbf{2})_2](PF_6)_2$ at 77 K. The weak, long-lived, high-energy emissions at λ_{max} 415−420 nm correspond to the calculated triplet absorptions and can be assigned as spin-forbidden π^*(Ph) → Au(d)−P(p) LMCT transitions. The

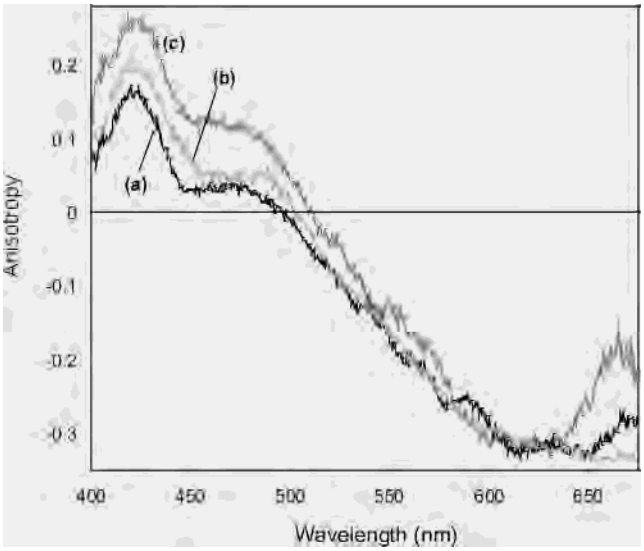

Figure 11. Luminescence anisotropy in ethanol at 77 K of (a) (±)-[Au_2-{(*R**,*R**)-**2**}$_2$](PF_6)$_2$, (b) [Au_2{(*R**,*S**)-**2**}$_2$](PF_6)$_2$, and (c) [Au(**1**)$_2$]PF_6.

intense, shorter-lived, lower-energy emissions at λ_{max} 520−595 nm are also observed at 293 K, where λ_{max} is 580−620 nm; these are the only emissions observed at ambient temperature. Because the energies of these transitions do not match the calculated ground-state absorptions for the cations, they appear to arise from new geometries for the cations in the excited state. Given the strong phenyl pairing for the complexes in their ground states, the most likely explanation for the differences must involve the formation of (Ph−Ph)* excited dimers. It is also possible that the differences arise from simple geometric relaxation in the triplet state, which can be >0.5 eV in such systems. The presence of excimers is, however, consistent with all the following observations: (i) the lower energy of the emissions relative to that of the calculated triplet, (ii) their substantially shorter lifetimes at 77 K relative to that of the triplet at λ_{max} 415−420 nm, (iii) the influence that the phenyl pairings in the ground state have on the excited-state lifetimes of these emissions, and (iv) the 5 nm red-shift in the excitation spectrum of these emissions at 77 K relative to those at λ_{max} 415−420 nm. On this basis, the emissions of the digold(I) and monogold(I) complexes at λ_{max} 520−595 nm are attributed to π*(Ph−Ph excimer) → Au(d)−P(p) LMCT transitions. The influence of simple geometric relaxation of the triplet state cannot be readily quantified.

Other Mechanisms. To test whether other assignments are consistent with these data, transitions centered on the ligands were examined. At 293 K, the free ligands **1** and (±)-(*R**,*R**)/(*R**,*S**)-**2** luminesce in the solid state at λ_{max} 440 nm with lifetimes in the nanosecond range. At 77 K in ethanol, the ligands emit weakly at 440 nm, with excitation spectra that match their absorption spectra but not those of the respective gold(I) complexes.

To determine whether the binding of the *P*-lone pairs could provide an alternative explanation, we also examined the luminescence of the protonated free ligands and the corresponding silver(I) complexes. At 293 K, the crystalline complexes [Ag(**1**)$_2$]PF_6, (±)-[Ag_2{(*R**,*R**)-**2**}$_2$](PF_6)$_2$, and

Scheme 3

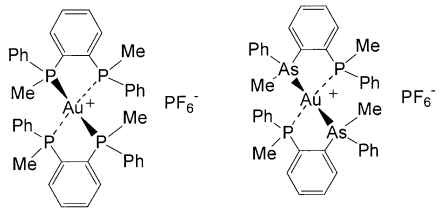

[Au(**5**)$_2$]PF_6 [Au(**6**)$_2$]PF_6

[Ag_2{(*R**,*S**)-**2**}$_2$](PF_6)$_2$ emit weakly at λ_{max} 469 nm and 395−415 nm, respectively. The complexes are also nonemissive in solution, emitting weakly in ethanol at 77 K at λ_{max} 435−470 nm, with negligible emissions in the region 500−600 nm (Figure 10). The protonated ligands emit at λ_{max} 395−415 nm at 77 K in ethanol and at 293 K. All of the emissions were too weak for accurate determinations of their lifetimes using the instrumentation available. The presence of gold(I) ions is therefore essential for luminescence, which is consistent with a mechanism involving an LMCT transition.

Another conceivable mechanism involves an excited state in which one Au−P bond is ruptured. Because three-coordinate Au(I) complexes are generally luminescent, the triplet excited state would be expected to display a considerable lifetime at low temperatures. This mechanism does not, however, offer an explanation for the observed solvent dependence, for the requirement that P−Ph groups be present, or for the apparent dependence on the phenyl pairings in the solid-state luminescence. Excimer formation is the simplest explanation consistent with these observations.

Other Au(I)−Phosphine Complexes. If the emissions observed for the mono- and digold(I) complexes arise from stacked *P*-Ph substituents and tetrahedral gold(I) ions, then other complexes containing these elements should also luminesce. The diastereomers of [Au(**5**)$_2$]PF_6 and [Au(**6**)$_2$]-PF_6, which also contain *P*-phenyl groups, produce distinct yellow luminescence when irradiated in the solid state, but not in solution (**5** = (*R**,*R**)/(*R**,*S**)-1,2-phenylenebis-(methylphenylphosphine); **6** = (*R**,*R**)/(*R**,*S**)-1-(methylphenylarsino)-2-(methylphenylphosphino)benzene) (Scheme 3).[25] Although the steady-state emission profiles of these complexes are comparable to those of [Au(**1**)$_2$]PF_6 and the digold(I) complexes, the emissions are less intense in the order [Au(**1**)$_2$]PF_6 > [Au(**5**)$_2$]PF_6 ≫ [Au(**6**)$_2$]PF_6. This result is in accord with a decreasing likelihood of *P*-Ph pairings in the crystals and the formation of *P*-Ph excimers.

Solution Structures. The complexes [Au(**1**)$_2$]PF_6 and [Au_2(**2**)$_2$](PF_6)$_2$ undergo rapid conformational flexing of chelate rings in solution. In CD_2Cl_2, this flexing occurs too rapidly to be resolved on the NMR time scale, even at −78 °C.[26] Excimer formation is likely to be hindered under such circumstances, thereby potentially explaining the non-

(25) (a) Roberts, N. K.; Wild, S. B. *J. Am. Chem. Soc.* **1979**, *101*, 6254. (b) Salem, G.; Wild, S. B. *Inorg. Chem.* **1983**, *22*, 4049.

(26) When cooled to −78 °C in CD_2Cl_2, the alkylene resonances of the digold(I) complexes display broad peaks in the ^{1}H NMR spectrum, indicative of rapid conformational flexing in solution (ref 5).

emissive nature of the mono- and digold(I) complexes in solution. Gold−phosphorus bond lability in solution may also explain the quenching of the emissions.[27]

Conclusions

Tetrahedral gold(I) complexes of the chelating di(tertiary phosphine) **1** and the tetra(tertiary phosphine) (*R**,*R**)-(±)/(*R**,*S**)-**2** luminesce with an intense yellow color (λ_{max} 580−620 nm) at 293 K in the solid state and when immobilized as molecular dispersions in solid matrixes. The Stokes shifts for these emissions are substantial, being 318 nm for [Au(**1**)$_2$]-PF_6 and 303 and 343 nm for the digold complexes, (±)-[Au_2{(*R**,*R**)-**2**}$_2$]$(PF_6)_2$ and [Au_2{(*R**,*S**)-**2**}$_2$]$(PF_6)_2$, respectively. The excited-state lifetimes of the emissions (τ 4.1−9.4 μs) appear to be dependent on inter- and intramolecular phenyl-group pairing interactions. At 77 K in an ethanol glass, two emissions are observed for all of the gold complexes: λ_{max} 415−450 nm (τ 251.0 ± 20.5 μs for [Au(**1**)$_2$]PF_6) and λ_{max} 520−595 nm (τ 14.9 ± 4.6 μs for [Au(**1**)$_2$]PF_6). Theoretical and comparative studies indicate that the former emissions comprise triplet LMCT $\pi^* \rightarrow$ Au(d)−P(p) transitions involving individual *P*-phenyl groups, while the latter involve LMCT π^*(Ph−Ph excimer) $\rightarrow$ Au(d)−P(p) transitions. The ligands, whether free, protonated, or bound to Ag(I), do not exhibit comparable emissions. Several other tetrahedral gold(I)−phosphine compounds containing *P*-phenyl substituents display similar emissions, suggesting luminescence to be general for this class of compounds. DFT calculations indicate that four-coordinate gold(I)−phosphine complexes not containing *P*-Ph or *P*-aromatic groups are unlikely to luminesce in the visible region.

Supporting Information Available: Full details of the X-ray crystal structure determination of (±)-[Au_2{(*R**,*R**)-**2**}$_2$]$(PF_6)_2$·2.77CH_2Cl_2·H_2O, including crystal data, details of data collection and refinement, tables of bond distances and angles, torsion angles, atomic coordinates and isotropic displacement parameters, anisotropic displacement parameters, geometric parameters, and contact distances (CIF and PDF). This material is available free of charge via the Internet at http://www.pubs.acs.org.

IC0206701

(27) (a) Palmer, J. A. L.; Wild, S. B. *Inorg. Chem.* **1983**, *22*, 4054. (b) Forward, J. M.; Assefa, Z.; Fackler, J. P. *J. Am. Chem. Soc*. **1995**, *117*, 9103.